Desalination and Water Treatment
www.deswater.com

doi: 10.1080/19443994.2015.1017008

57 (2016) 7387–7395
April

Taylor & Francis
Taylor & Francis Group

Comparable phosphate adsorption onto some natural aluminosilicates vs. Fe(III)oxihydroxide

Eva Chmielewská[a,*], Renata Hodossyová[a], Mária Koval'aková[b], Martin Urík[a]

[a]*Faculty of Natural Sciences, Comenius University, Mlynská dolina, 842 15 Bratislava, Slovak Republic, Tel. +421 26 029 64 10; emails: chmielewska@fns.uniba.sk (E. Chmielewská), rhodossy@gmail.com (R. Hodossyová), martin.urik@gmail.com (M. Urík)*
[b]*Faculty of Electrical Engineering and Informatics, Technical University of Košice, Park Komenského 2, 042 00 Košice, Slovak Republic, Tel. +421 55 602 28 32; email: maria.kovalakova@tuke.sk*

Received 8 July 2014; Accepted 1 February 2015

ABSTRACT

In this paper, the attention was focused on the phosphate removal using the various, mostly traditional or naturally available adsorbents, few of the local repositories, which prove enhanced performance for phosphate removal. The highest capacity toward phosphate ions showed montmorillonite and Fe-oxihydroxide (GEH), while the uptake capacity of slovakite and clinoptilolite-rich tuff was about 30% lower. In dynamic regime, the best performance in phosphate uptake proved GEH. The experimentally recorded breakthrough curves were mathematically described by Yan and Thomas models. Their empirical equations were found to satisfactory describe the breakthrough curves in a fixed bed column ($R^2 > 0.92$); however, the both models approached to the experimentally obtained adsorption capacity data more or less only for zeolite column. The highest elution of phosphate into tap water was observed by montmorillonite (about 50%), while by clinoptilolite-rich tuff the elution using the tap water was rather low. MAS NMR measurements confirmed that mostly Ca^{2+} cations occurring in clinoptilolite-rich tuff framework dominate in $Ca_3(PO_4)_2$ surface precipitation.

Keywords: Clinoptilolite-rich tuff; Fe-oxihydroxide (GEH); Slovakite; Montmorillonite; Phosphate removal; Precipitation; Complexation; Elution; Isotherm

1. Introduction

At the end of the nineteenth century, biological treatment of wastewater accounted mostly for organic matter (biological oxygen demand) removal and had not significantly progressed beyond until that time. Several alternative physicochemical methods like flocculation and phosphate adsorption using alum or iron oxihydroxides with lime precipitation were simultaneously developed. At this time, phosphorus removal from the wastewater had neither been considered an important issue and until the 1950s nor scientifically researched [1].

In the United States of America, during the WW II, some efforts had been undertaken to precipitate phosphorus from wastewater to produce agriculture fertilizer, due to dramatic shortages of mineral apatites that were imported up to that time from North Africa. Better understanding of natural principles of eutrophication ongoing in surface waters were initiated first by Rudolfs and later by Lea with his co-workers to propose an advanced, more effective bioprocess for phosphorus removal [1].

*Corresponding author.

In Switzerland, in 1960, chemical precipitation of phosphate in front of a primary clarifier within a conventional biological wastewater treatment plant was carried out. Similarly, in Scandinavian countries, where chemicals have been dosed, this was done but instead of in front of the primary clarifier, it was sent directly to the activated sludge process [2].

Levin and Shapiro [3] reported the removal of phosphorus by means of a sludge activation process exposing the phosphorus for removal in sequential aerobic and anaerobic conditions. Both observed that the exceeded phosphorus uptake was realized within photosynthesis. They initially called this phosphorus uptake, especially under aerobic conditions, "luxury uptake" and characterized this process as reversible, despite not having a clear understanding of the process. Nevertheless, taking into account those observations, the basis for what would later be called the Phostrip process was established.

A modern multiphase biological reactor, working as an integrated phosphorus and carbon removal plant, was developed by Barnard [4]. He appears to have improved and modified the treatment design according to Wuhrmann. Barnard constructed a reactor with an inner recirculation system where mixed liquids were directed from the final zone of the aerobic process to the anaerobic chamber, while phosphorus was released under anaerobic conditions.

Today, the main sources of phosphorus are produced mostly from human excreta (30–50%), detergents (50–70%), and industry (2–20%). Influencing the human excreta load is, at best, difficult to manage, therefore public and governmental pressure to minimize the phosphorus contained in household detergents was initiated in the 1970s. More recently, in 2013, the European Union passed legislation prohibiting phosphate detergents use based upon their compound influence for algae and red tide growths in waters [5,6].

According to the report by Rybicki [1], orthophosphate is the predominate phosphate in all waters by more than 50%, while organic phosphorus and polyphosphate species represent considerably lower concentrations. Because the phosphorus in wastewater was present in a soluble form, all the older applied methods for phosphorus removal were based on the general principle of converting soluble phosphorus into non-soluble one, i.e. either as precipitated compounds or as phosphorus built-in to micro-organisms by subsequent separation of both [7].

Prospects for improvements to current phosphorus removal would be such (i) to ensure the easily biodegradable carbon source, (ii) to ensure genetically engineered micro-organisms, (iii) to provide fully anaerobic conditions in the anaerobic zone of bioreactor, (iv) to setup the *predenitrification* to remove nitrates from the raw wastewater and after those various scenarios have been optimizated, and (v) to supply the plant with the automated process control.

For the complementary or tertiary removal of phosphorus from the wastewater in other words, subsequent polishing steps, the following recently suggested ideas have included (i) exposing the open culture of algae (*Phormidium bohneri, Chloral vulgarize*), (ii) waste ponds, or (iii) artificial wetland, because only a small percentage of the total phosphorus is expected to be removed by harvested plants, due to phosphorus accumulation mostly in the roots [1,8].

Natural materials like clay, limestone, and waste by-products from industrial processes, e.g. water treatment residuals (alum sludge), fly ash, and iron or steel slags have been studied for remediation of a wide range of contaminants incl. orthophosphate in waters [9]. The reuse of waste by-products for beneficial purpose, such as water treatment, is attractive as an alternative to disposal. Also some engineered adsorption materials, like Fe(III)-immobilized polymer anion exchange resin, Fe(III)-immobilized porous silica, iron oxide-coated fungal biomass, chitosan/bentonite composite or synthetic goethite, and akaganeite were successfully used for phosphate removal out of the various types of water [7–10].

In this paper, attention was focused on the various traditional adsorbents, few of the local repositories, which showed enhanced performance for phosphate removal. Due to their low-cost and local availability, natural materials such as zeolite, montmorillonite, dolomite, clay, and iron oxihydroxides were chosen to evaluate their adsorption performance in both batch- and dynamic-scale experiments. The elution strength of such surface-adsorbed complexes was examined, respectively. Moreover, ^{31}P MAS NMR measurements have been carried out to verify the presence of adsorbed orthophosphate onto clinoptilolite-rich tuff, montmorillonite, and slovakite.

2. Materials and methods

2.1. Adsorbents examined for phosphate removal

Granulated ferric hydroxide (GEH^{104}), developed at the Department of Water Quality Control in Technical University Berlin, is an approved commercial adsorbent manufactured by Fe-oxihydroxide (GEH) Wasserchemie GmbH & Co. KG Osnabrück (Germany). The main components of GEH are akaganeite (ß-FeOOH) and goethite [α-FeO(OH)]. The product has the specific surface area about 220 $m^2 g^{-1}$, water content of 45%,

bulk density 1.2 g cm^{-3}, and the price of 3,750 Euro per ton [10].

The domestic clinoptilolite-rich tuff (deposit Nižný Hrabovec at the eastern Slovakia) was chosen on the base of its low-price availability in the local market (15–35 Euro per ton for size granulation of 0.3–1 mm), cost effectiveness, and due to its sufficiently large surface area (~60 $m^2 g^{-1}$), the highest one among the other natural products, rigidity, and surface functionality [11–17]. **Slovakite** decodes a commercial adsorbent manufactured by IPRES inžiniering, Ltd. Bratislava from domestic dolomite, bentonite, diatomic clays, alginite, and zeolite, justified only with clinker and final pressurizing. Slovakite is purchased for about 700 Euro per ton. The bulk density of this product equals 2.1 g cm^{-3} and S(BET) surface to 23 $m^2 g^{-1}$ [11].

The Al–Mg—Montmorillonite-rich bentonite originated from the deposit Stará Kremnička-Jelšový Potok in the Slovak Republic, which is the most popular and long mined ore of the country. Montmorillonite from the montmorillonite-rich bentonite was obtained after sedimentation and purification procedures. The price of the montmorillonite on the market ranges in 30–80 Euro per ton. Its surface area S(BET) reaches the value 240 $m^2 g^{-1}$, and the bulk density of montmorillonite is about 2.0 g cm^{-3} [11].

2.2. Experimental setup and analytical determination

Chemicals necessary for the stock solution preparation were purchased mostly from Lachema Brno (made in Czech Republic) with analytical-grade quality. For the experiments, the deionized (DI) water was used for preparation of the model phosphate solution, which pH value was lower than 7 just a little. Aqueous model solutions of the pollutant examined in adsorption experiments (as phosphate) were determined by means of atomic emission spectrometry (ICP OES, Jobin Yvon 70 Plus) at the wavelength 213.618 nm for phosphorus.

To compare all the above materials with each other, continuous or mini-column experiments were firstly realized in glass tubes with inner diameter of 20 mm and height of 300 mm, where the adsorbent weight, i.e. bed volume (BV) of 30 mL reached approx. 20 g. Each adsorbent with the grain size of 0.5–1.0 mm was filled over about 1–2 mL support layer of glass fiber. To minimize the clogging of the columns, the column setup was cleaned with DI water before each experiment. Water was pumped down-flow through the column at the flow rate of 2.5–5 mL min^{-1} (5–10 BV h^{-1}), by keeping the constant height of column level and thus providing the uniform hydrostatic pressure. Samples of filtered water were collected and analyzed at pre-determined times over the whole experiment duration, by gradually approaching the total column saturation.

The column flow data were evaluated using the Yan and Thomas models by non-linear regression analysis with the software package STATISTICA (Release 5.0) for Windows.

Also well-mixed batch reactor was actually accomplished by using the RS-60 BioSan (Lithuania) multirotator, which plastic tubes were filled with measured adsorbent suspensions according to the conventional batch procedure.

The ^{31}P MAS NMR measurements were performed using the pure $Na_3PO_4{\cdot}12H_2O$ chemical, respectively, which was used in the adsorption experiments and pure $NH_4H_2PO_4$, which was applied as an external standard. The ^{31}P measurements were carried out on 400 MHz Varian Spectrometer (USA) with a superconducting wide-bore magnet, generating a magnetic field of 9.4 *T*, at room temperature by using a probehead with 4 mm rotor spinning and at magic angle with rate of 10 kHz (resonance frequency of 161.646 MHz, 90º pulse duration of 3.8 μs, and recycle delay 300 s). The spectra were processed with the MestReNova software.

3. Results and discussion

Adsorption kinetics were determined for clinoptilolite-rich tuff, slovakite, montmorillonite, and GEH in aqueous phosphate solutions for adsorption isotherm computation and the plotting of chronological pH–time dependence as illustrated in Fig. 1. Adsorption equilibrium was reached faster on montmorillonite and slovakite than by the clinoptilolite-rich tuff and Fe-oxihydroxide. Based upon these results, a 4 h interval was sufficient to achieve steady-state conditions. The highest capacities for phosphate ions were those of montmorillonite and GEH. Nevertheless, the capacity of clinoptilolite-rich tuff toward phosphate was estimated as competitive. Any chronological change of pH in suspensions with clinoptilolite-rich tuff and slovakite was negligible whereas in montmorillonite and Fe-oxihydroxide, a pH decrease corresponded to phosphate uptake. This related to the gradual removal of anions from the solution phase.

A continuous, well-mixed, batch reactor was used to compare the adsorption performance of the four materials. Such experimental configuration offers a number of potential advantages such as long contact times, upon which a high particle load used to be derived or controlled the mixing to reduce an external mass-transfer effect.

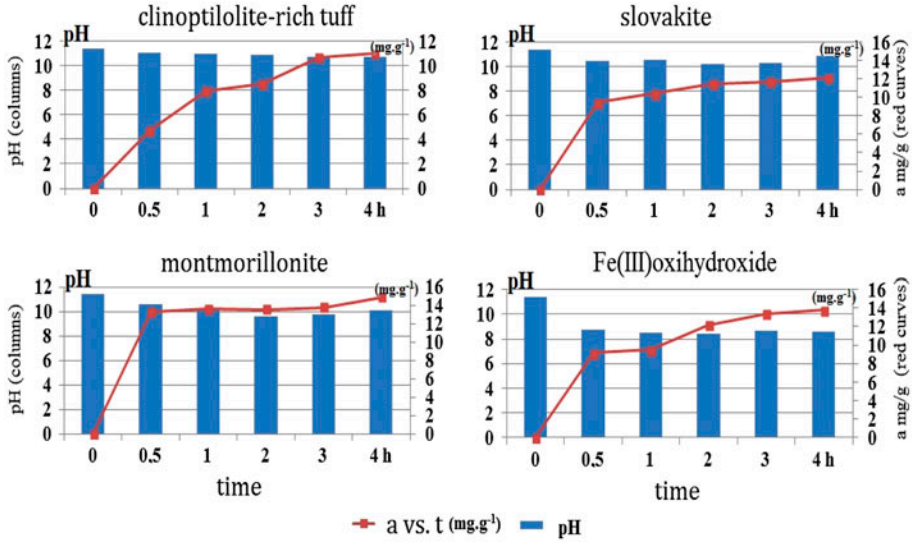

Fig. 1. Adsorption kinetics (red curves) onto 4 adsorption materials in phosphate solutions incl. pH vs. time dependence.

Based upon the batch mode experiments, the highest phosphate removal was reached by montmorillonite and GEH, while the uptake capacity of slovakite and clinoptilolite-rich tuff was about 30% lower (Fig. 2). The mathematical description of the isotherms calculated was as published in the literature [11].

In the dynamic regime, the best performance in phosphate uptake proved to be that of GEH based on its symmetric near S-shaped breakthrough curve, while the curves of zeolite and slovakite proved too short and had prolonged fronts to the adsorption zones, probably due to an insufficient residence time of the solute in packed beds (about 3–5 min), i.e. too short to achieve equilibrium (Fig. 3a). Montmorillonite was not examined in these mini-columns experiments due to its poor hydrodynamic property.

Table 1 summarizes all the dynamic parameters of the mini-column experiments accompanied by the mathematical description of the breakthrough curves using Yan and Thomas models (Table 1, Fig. 3b), where $k_{Y,}$ k_{Th} are the kinetic rate constants for the Yan or Thomas models (L h^{-1} mg^{-1}), $a_{Y,}$ a_{Th} are the adsorption capacities estimated by Yan or Thomas models (mg g^{-1}), Q is the volumetric flow (L h^{-1}), and m is the adsorbent weight (g). These empirical equations proposed by Yan et al. [18] and Thomas [19] were found to satisfactory describe the breakthrough curves in a

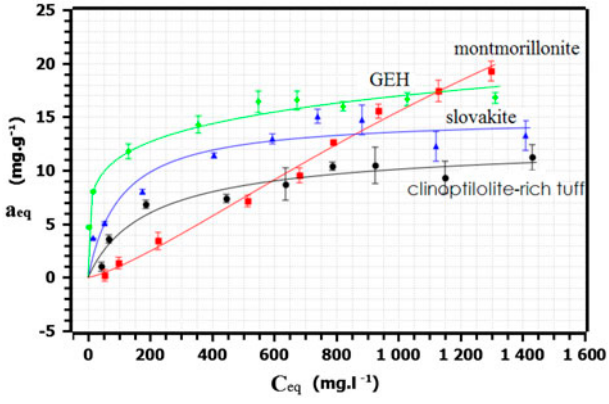

Fig. 2. Adsorption isotherms measured for the system orthophosphate solution vs. GEH, clinoptilolite-rich tuff, montmorillonite, or slovakite at $T = 23 \pm 0.2$°C (a_{eq} equilibrium adsorption capacity, c_{eq} equilibrium concentration).

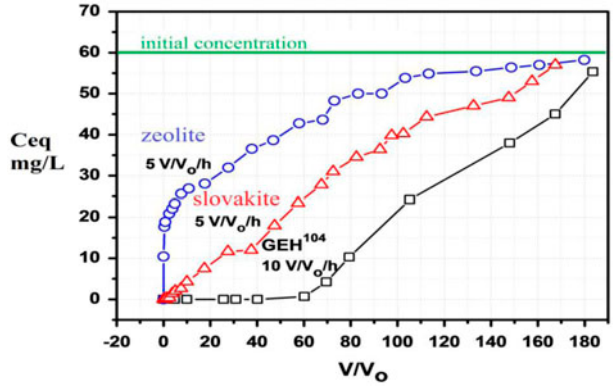

Fig. 3a. Column runs onto the examined adsorbents (except the montmorillonite) using the phosphate solution of initial concentration $C_o = 60$ mg L^{-1} and the experimental data (V/Vo/h = BV h^{-1}—flowrate).

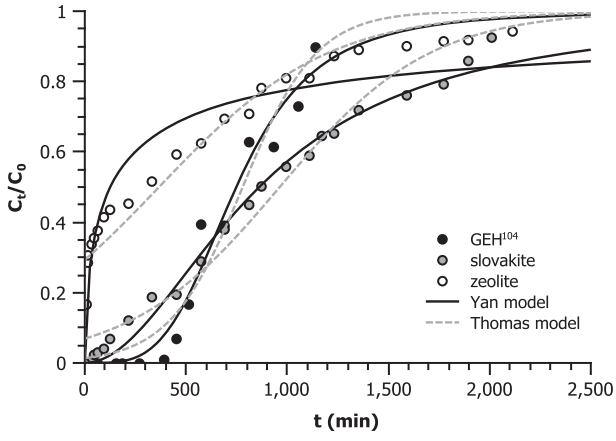

Fig. 3b. Column runs onto the examined adsorbents (except the montmorillonite) using the same phosphate solution and the data computed according to Yan and Thomas models.

fixed bed column ($R^2 > 0.92$). The Yan model also predicted the effluent concentration at time zero.

The dynamic adsorption capacity is the capacity of the adsorbent in the column at the time when the first leakage with the limited pollutant concentration in the effluent appeared. The static adsorption capacity was measured at the moment when the pollutant concentration in effluent of the column reached the pollutant influent concentration, i.e. the column was saturated with the pollutant. Maximum adsorption capacity was extrapolated from the recorded isotherms (Fig. 2). These capacity values were expressed per gram of dried adsorbent (Table 1). As can be seen from Table 1, the adsorption capacities according to Thomas model differed from the static adsorption capacities measured during the lab trials and calculated volumetrically (recorded as a_{stat}, using the influent concentration of $C_0 = 60$ mg L^{-1}) by 20 and 28% for zeolite and GEH columns, and the computed slovakite capacity differed by 48%. Using the Yan model, only the computed zeolite column capacity was the most comparable to the experimental adsorption capacity a_{stat} (19% difference). In other words, the both models approached to the experimentally obtained data only for zeolite column. Thus, the restrictions in a_{Th}, a_Y computation seemed to be mostly in the column concentration profiles which indicated the highest effectivity during the solid bed filtration.

The differences in uptake capacities between the selected adsorbents may be explained as follows: the phosphate adsorption onto clinoptilolite-rich tuff proceeds by the mechanism of surface accessible extra-framework cations Ca^{2+} and Mg^{2+} enabling calcium

Table 1
Dynamic parameters of mini-column experiments incl. mathematical description of breakthrough curves according to Yan and Thomas models (a_{dynam}—dynamic adsorption capacity; a_{max}—maximum adsorption capacity (total, extrapolated from isotherm); a_{stat}—static adsorption capacity or saturation capacity by the identical influent concentration)

	Adsorption capacity estimated by the Yan model (mg g^{-1})	Yan model rate constant (L h^{-1} mg^{-1})	R^2	Yan model $\frac{C_t}{C_0} = 1 - \frac{1}{1 + \left(\frac{Q^2 t}{k_Y a_Y m}\right)^{(k_Y C_0/Q)}}$	Experimental capacity (mg g^{-1})		
					a_{dynam}	a_{max}	a_{stat}
GEH	1.82 ± 0.18	0.011	0.97	$\frac{C_t}{C_0} = 1 - \frac{1}{1 + (1.33 \times 10^{-3} t)^{3.8}}$	2.84	18	10
Slovakite	3.37 ± 0.16	0.005	0.99	$\frac{C_t}{C_0} = 1 - \frac{1}{1 + (1.16 \times 10^{-3} t)^{1.97}}$	2.12	14	5
Zeolite	1.36 ± 0.19	0.001	0.93	$\frac{C_t}{C_0} = 1 - \frac{1}{1 + (7.9 \times 10^{-3} t)^{0.6}}$	1.14	11	3
Montmorillonite						20	0.9
	Adsorption capacity estimated by the Thomas model (mg g^{-1})	Thomas model rate constant (L h^{-1} mg^{-1})	R^2	Thomas model $\frac{C_t}{C_0} = \frac{1}{1+\exp\left[\left(\frac{k_{Th} a_{Th} m}{Q}\right) - k_{Th} C_0 t\right]}$			
GEH	7.21 ± 0.21	0.005	0.96	$\frac{C_t}{C_0} = \frac{1}{1 + \exp(4.29 - 0.0055t)}$			
Slovakite	7.45 ± 0.21	0.003	0.97	$\frac{C_t}{C_0} = \frac{1}{1 + \exp(2.60 - 0.0027t)}$			
Zeolite	2.41 ± 0.24	0.002	0.92	$\frac{C_t}{C_0} = \frac{1}{1 + \exp(0.88 - 0.0024t)}$			

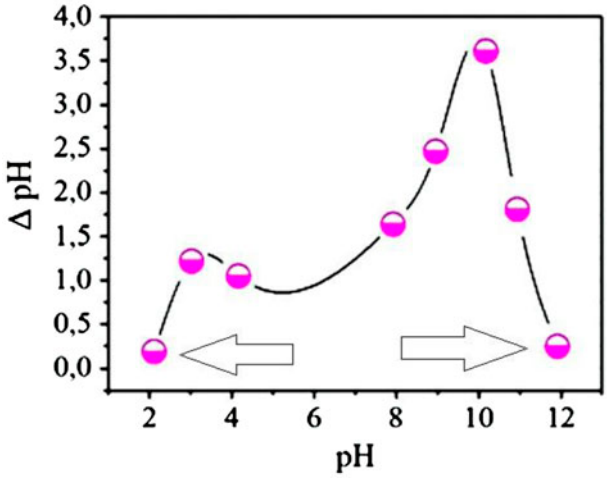

Fig. 4. The point of zero charge measurements using the salt addition method for natural zeolite clinoptilolite.

and magnesium phosphates precipitation. Adsorption onto GEH proceeds by means of linkage of phosphate anions to the Fe^{3+} cations of the akaganeite structure, probably by much stronger covalent bonding. It must be pointed simultaneously, that the clinoptilolite tuff, who's zeolite framework contains narrow 4− and 5−membered SiO_4^{4-} and AlO_4^{5-} tetrahedral rings as well as broad 8- and 10-membered tetrahedral rings constituting intra-framework micropores (channels) of 0.33 × 0.46 nm, 0.3 × 0.76 nm, and 0.26 × 0.47 nm dimensions, enriched by mobile H_2O molecules, also contains due to the presence of other minerals overgrowing the active matrix (such as volcanic glass, feldspar, cristobalite, clay, and quartz), much broader external pore openings and various interparticle voids, which probably act as phosphate scavengers. Based on the S (BET) analyses performed, the BJH average pore diameters of the clinoptilolite sample was in the range of 9.2–20 nm. On the basis of the ionic diameter of non-hydrated PO_4^{3-}, i.e. 1.196 nm, only interlamellar space of the montmorillonite structure (interlayer distance of about 1.2 nm) approaches this dimension and thus potentially supports a phosphate intercalation mechanism by this process [20]. Finally, phosphate adsorption onto slovakite is assumed to proceed again by linkage of phosphate to the alkaline-earth cations occurring in its dolomite and clay constituents. The much smaller GEH surface area meant that slovakite was a less effective adsorption material than GEH.

Fig. 4 records two measured zero charge points for clinoptilolite-rich tuff, which indicated the most appropriate pH values for adsorbate immobilization onto the zeolitic surface. Uptake has been confirmed for other anions, such as chromate, arsenate, nitrate, sulfate, etc. However, for our experiments, deionized

Table 2
Results of elution tests by various chemicals incl. cationic contents of bulk phases measured by EDX

Adsorbent	Zeolite			GEH[104]			Slovakite			Montmorillonite		
Elutions (mg L^{-1})	Ca	Mg	Fe	Ca	Mg	Fe	Ca	Mg	Fe	Ca	Mg	Fe
In 1% NH_4Cl	82.13	6.91	0.04	6.69	1.25	0.03	134.7	85.68	0.02	42.84	7.95	21.12
In deionized H_2O	3.17	0.82	0.41	5.21	1.22	6.49	5.37	1.37	0.03	37.38	14.1	0.35
EDX (%)	0.95	0.9	8.67	0.13	1.5	37.6	31.13	1.2	2.01	1.21	3.65	1.54
Efficiency (%) 1% NH_4Cl/elutions	86	7.6	0.004	51.3	8.2	$7.9.10^{-4}$	4.34	71.4	0.009	35.4	2.1	13.7
Efficiency (%) deion. H_2O/elutions	3.3	0.91	0.04	40	8.1	0.17	0.17	1.13	0.014	30.8	3.8	0.2
Dephosphatization in NH_4Cl	a_m (PO_4^{3-}) 12 mg g^{-1}	Elution/NH_4^+ 16.6%		a_{max} (PO_4^{3-}) 19 mg g^{-1}	Elution/NH_4^+ 2.1%		a_m (PO_4^{3-}) 16 mg g^{-1}	Elution/NH_4^+ 2.5%		a_{max} (PO_4^{3-}) 22 mg g^{-1}	Elution/NH_4^+ 50%	

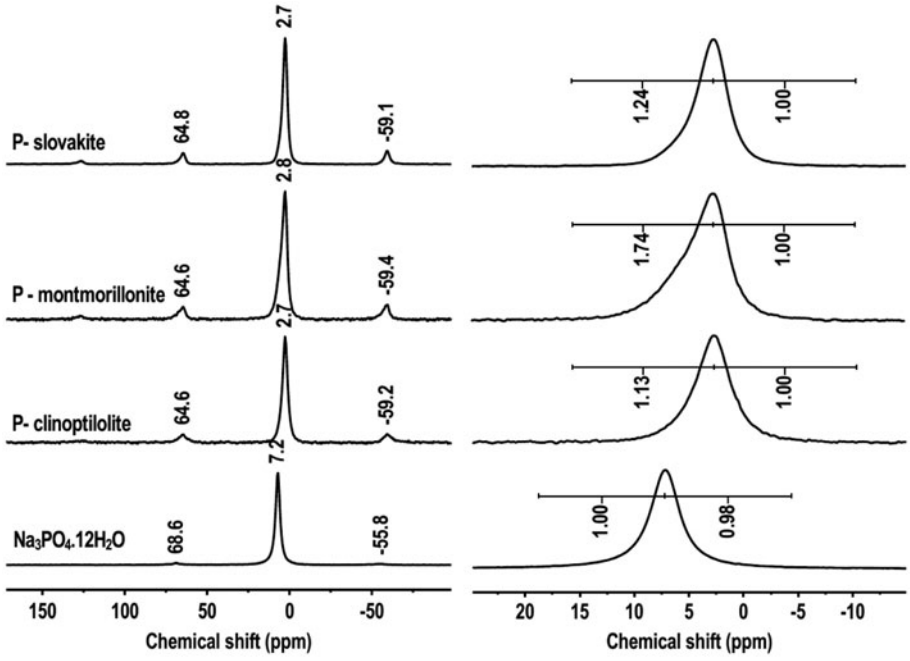

Fig. 5. (a) ^{31}P MAS NMR spectra of $Na_3PO_4{\cdot}12H_2O$, phosphatized, i.e. P-clinoptilolite, P-montmorillonite, and P-slovakite (upwards), (b) ^{31}P MAS NMR spectra with integrals of the symmetric intervals in respect to central line.

Table 3
Deconvolution ^{31}P MAS NMR spectra of phosphatized clinoptilolite-rich tuff, montmorillonite, and slovakite

Phosphatized adsorbent	δ_{iso} (ppm)	Compounds	% Areal extent
Montmorillonite	2.8	$Ca_3(PO_4)_2$	67.2
	5.8	$Mg_3(PO_4)_2{\cdot}8H_2O$	27.4
Clinoptilolite-rich tuff	2.7	$Ca_3(PO_4)_2$	95
Slovakite	2.7	$Ca_3(PO_4)_2$	85
	5.6	$Mg_3(PO_4)_2{\cdot}8H_2O$	15
GEH	–	–	–

water was used for preparation of the phosphate solutions, which had pH values just less than 7 [21].

To compare the bonding strengths of the adsorbed phosphate on the four best adsorbents, i.e. clinoptilolite-rich tuff, GEH, montmorillonite, and slovakite, some simple tests for reversed elution of phosphate into 1% NH_4Cl solution and tap water was realized. Before this elution test, all adsorbents were loaded with phosphate by an identical procedure in aqueous solutions of 100 g PO_4^{3-}/L (10 g of adsorbent in 1 L of solution) using the laboratory shaking machine for 4 h. Phosphate-loaded adsorbents were separated and thoroughly washed in deionized water to remove weakly bonded phosphate from the sand and then dried at 105°C for 2 h in laboratory drier.

As can be seen at Table 2, the highest elution was that from montmorillonite (about 50%), while for clinoptilolite-rich tuff, the elution with tap water was low; however, the elution with 2% ammonium chloride was considerable higher—16.6%, probably on the basis of zeolitic strong selectivity toward ammonium ion. The lowest elutions were exhibited by GEH and slovakite (2.1–2.5%). According to the EDX analysis, the most desorbed element was calcium (up to 86% into ammonium chloride). About 31% of calcium and ca. 14% of the total iron of their contents in the parent solid samples were desorbed or washed out within 4 h from the phosphatized montmorillonite (Table 2).

Finally, ^{31}P MAS NMR measurements have been carried out to verify the presence of adsorbed phosphate onto clinoptilolite-rich tuff, montmorillonite, and slovakite (at Fig. 5 denoted as P-clinoptilolite, P-montmorillonite, and P-slovakite). The ^{31}P MAS NMR spectra of all samples are characterized by one

central signal with symmetrically positioned spinning sidebands (Fig. 5(a)). Chemical shift of the central line in the spectrum of $Na_3PO_4{\cdot}12H_2O$ is by 0.4 ppm lower than the value reported in the literature [22], caused probably by partial hydration of sample. Chemical shifts of central lines in the spectra measured for particular adsorbents are of 2.7–2.8 ppm, however, in a good agreement with the value of 2.8 ppm published for pure $Ca_3(PO_4)_2$ [22,23]. Based upon that results, dominant signal at chemical shift of 2.7–2.8 ppm may be assigned as surface precipitate $Ca_3(PO_4)_2$. According to Fig. 5(b), the central signals in the spectra of adsorbents are not symmetrical. Such asymmetry can be quantified by integration of two symmetrical intervals in regard to the center of measured data. Pure $Na_3PO_4{\cdot}12H_2O$ proves a symmetric signal, and both the left and right integral values are the same. In the case of phosphatized adsorbents, the left integrals were always larger than the right ones, while the largest asymmetry was observed by P-montmorillonite. Based upon that fact, PO_4^{3-} anions may react not just with Ca^{2+} but also very likely with other cations, such as Al^{3+}or Mg^{2+}, which are probably present in the outer pores of mineral and thus form compounds with a higher ^{31}P chemical shift. However, the best symmetry in the spectrum of P-clinoptilolite indicated that Ca^{2+} cations are those most frequently occurring in clinoptilolite-rich tuff framework.

The most asymmetric signals in the spectrum of P-montmorillonite was deconvoluted into three lines and in the spectrum of P-slovakite into two lines with Lorentzian/Gaussian ratio. The results of deconvolutions are listed in Table 3. The area (line intensity) is proportional to the amount of precipitate.

4. Conclusion

Based upon the experimental results obtained in this study, following conclusions may be stated:

The commercial products (GEH and slovakite) and the domestic natural clinoptilolite-rich tuff and montmorillonite adsorbents in laboratory-scale were examined for phosphate removal.

The adsorption equilibrium in the systems studied was reached faster by montmorillonite and slovakite than by the clinoptilolite-rich tuff and Fe-oxihydroxide. Based upon these results, the 4 h interval was sufficient to achieve the steady-state conditions, while the highest capacities toward phosphate ions were observed for montmorillonite and GEH, while the uptake capacity of slovakite and clinoptilolite-rich tuff was about 30% lower.

In the dynamic regime, the best performance in phosphate uptake proved to be GEH judged by its symmetric, almost S-shaped breakthrough curve, while those of zeolite tuff and slovakite proved to have short and prolonged fronts to their adsorption zones. The experimentally recorded breakthrough curves were mathematically described by Yan and Thomas models.

The two zero charge points (pH 2 and 12) for clinoptilolite-rich tuff indicated the most appropriate pH values for adsorbate immobilization onto zeolitic surface.

The highest elution of phosphate into tap water was observed by montmorillonite (about 50%), whereas for the clinoptilolite-rich tuff elution using the tap water was rather low. On the other hand, easier desorption of precipitates of calcium and magnesium phosphates from the surface of clinoptilolite-rich tuff into 1% NH_4Cl solutions was found. The desorption of phosphate linked to the surface of GEH, as well as phosphate linked to the alkaline-earth cations of the slovakite provided considerable lower desorption efficiencies, i.e. desorption of phosphate from the GEH was qualitatively about three times lower than the clinoptilolite-rich tuff.

According to MAS NMR measurements, the best symmetry among the recorded spectra was that of the P-clinoptilolite sample, supporting the presumption that Ca^{2+} cations occurring in clinoptilolite-rich tuff framework dominate in $Ca_3(PO_4)_2$ surface precipitation.

Thus, based upon the zeolite competitive effectivity, the economic feasible clinoptilolite-rich tuff may be considered as the best potential candidate for phosphate removal from water.

Acknowledgement

This project was funded by the Slovak Scientific Council VEGA (Project # 1/0250/15) and by Agency for Science and Research (APVV) under Project # SK-CN-0033-12.

References

[1] S.M. Rybicki, Advanced wastewater treatment: Phosphorus removal from wastewater, A literature review, Joint Polish-Swedish Report, Kungl Techniska Högskolan, Stockholm, 1997, pp. 106–140.
[2] P. Balmer, B. Hultman, Control of phosphorus discharges: Present situation and trends, Hydrobiologica 170 (1988) 305–319.
[3] G.V. Levin, J. Shapiro, Metabolic uptake of phosphorus by wastewater organisms, J. Water Pollut. Control Fed. 37 (1965) 800–807.
[4] J. Barnard, Background to biological phosphorus removal, Water Sci. Technol. 15 (1983) 1–13.

[5] EU Directive No. 259/2012, Phosphate and phosphorus contained substances limitation in households detergents. Available from: http://enviroportal.sk.
[6] WHO, Guidelines for Drinking Water Quality, fourth ed., WHO Press, Geneva, 396–397, 2011.
[7] S.A. Gobbi, F.B. Filho, Reduction of environmental pollution caused by phosphate through the use of natural zeolite (clinoptilolite) production of powder detergents, in: Zeolite 2010—8th Int. Conf. Occurrence, Properties and Utilization of Natural Zeolites, Sofia Bulgaria, 10–18 July 2010, pp. 97–98.
[8] T.H. Boyer, A. Persaud, P. Banerjee, P. Palomino, Comparison of low cost and engineered materials for phosphorus removal from organic-rich surface water, Water Res. 45 (2011) 4803–4814.
[9] G. Rezmi, I. Buddhima, L.D. Nghiem, L. Banasiak, Evaluating waste concrete for the treatment of acid sulphate soil ground water from coastal floodplains, Desalin. Water Treat. 32 (2011) 126–132.
[10] P. Weiss, Die Entwicklung Eisenhydroxid Reaktors zur Phosphateliminierung (Development of iron oxihydroxide reactor for phosphate removal), GWF. Wasser Abwasser. 133(9) (1992) 583–587.
[11] E. Chmielewská, R. Hodossyová, M. Bujdoš, Kinetic and thermodynamic studies for phosphate removal using natural adsorption materials, Pol. J. Environ. Stud. 22(5) (2013) 1307–1316.
[12] C. Hårleman, G. Jacks, B. Rybeck, The use of a clinoptilolite-based filter in emergency situations, Desalination 248 (2009) 629–635.
[13] S. Wang, Y. Peng, Natural zeolites as effective adsorbents in water and wastewater treatment, Chem. Eng. J. 156 (2010) 11–24.
[14] L. Liberti, G. Boghetich, A. Lopez, D. Petruzelli, Application of microporous materials for the recovery of nutrients from wastewaters, in: P. Misaelides, C. Colella (Eds.), Natural Microporous Materials in Environmental Technology, Kluver Academic Publishers, Dordrecht, 1999, pp. 253–269.
[15] E. Sánchez, Z. Milán, R. Borja, P. Weiland, X. Rodrigues, Piggery waste treatment by anaerobic digestion and nutrient removal by ionic exchange, Resour. Conserv. Recycl. 15 (1995) 234–244.
[16] A. Lopez, L. Liberti, Zeolites "closed-loop" regeneration, in: C. Colella (Ed.), Atti 1st Convegno Nazionale di Scienza e Tecnologia delle Zeoliti, L´Aquila 26–27 Settembre, 1991, pp. 139–146.
[17] V. Amicarelli, L. Liberti, Zeolite ammonia removal at Manfredonia municipal plant, in: C. Colella (Ed.), Atti 1st Convegno Nazionale di Scienza e Tecnologia delle Zeoliti, L´Aquila 26–27 Settembre 139–146, 1991, pp. 147–155.
[18] G. Yan, T. Viraraghavan, M. Chen, A new model for heavy metal removal in a biosorption column, Adsorpt. Sci. Technol. 19(1) (2001) 25–43, doi: 10.1260/0263617011493953.
[19] H.C. Thomas, Heterogeneous Ion Exchange in a Flowing System, J. Am. Chem. Soc. 66 (10) (1944) 1664–1666, doi: 10.1021/ja01238a017.
[20] K. Barbalace, Periodic Table of Elements—Sorted by Ionic Radius. Environmental Chemistry.com, 1995–2010. Available from: http://klbprouctions.com (accessed 2010-7-03).
[21] S. Mustafa, B. Dilara, A. Nargis, A. Naeem, P. Shahida, Surface properties of the mixed oxides of iron and silica, Colloids Surf., A 205 (2002) 273–282.
[22] Z. He, C.W. Honneycutt, T. Zhang, P.J. Pellechia, W.A. Caliebe, Distinction of Metal Species of Phytate by Solid-State Spectroscopic Techniques, SSSAJ. 71 (2007) 940–943.
[23] M. Kovalaková, E. Chmielewská, R. Hodossyová, V. Hronský, P. Duranka, Solid state NMR of phosphate adsorption on natural microporous materials, Applied Physics of Condensed Matter, 18th Int. Conference 20–22 June 2012. Štrbské Pleso, Proceed. (ISBN 978-80-227-3720-3).